THE JOURNAL OF BIOLOGICAL CHEMISTRY
Vol. 278, No. 45, Issue of November 7, pp. 44600–44607, 2003
Printed in U.S.A.

Crystal Structure and Functional Analysis of *Drosophila* Wind, a Protein-disulfide Isomerase-related Protein*[S]

Received for publication, July 22, 2003
Published, JBC Papers in Press, August 26, 2003, DOI 10.1074/jbc.M307966200

Qingjun Ma‡§, Chaoshe Guo§¶, Kathrin Barnewitz¶, George M. Sheldrick‡, Hans-Dieter Söling¶, Isabel Usón‡, and David M. Ferrari¶‖

From the ‡Department of Structural Chemistry, University of Göttingen, Tammanstrasse 4 and the ¶Department of Neurobiology, Max Planck Institute of Biophysical Chemistry, Am Fassberg 11, D-37077 Göttingen, Germany

In the developing *Drosophila melanogaster* embryo, dorsal-ventral patterning displays an absolute requirement for the product of the essential *windbeutel* gene, Wind. In homozygous *windbeutel* mutant flies, dorsal-ventral patterning fails to initiate because of the failure of the Golgi-resident proteoglycan-modifying protein, Pipe, to exit the endoplasmic reticulum, and this leads to the death of the embryo. Here, we describe the three-dimensional structure of Wind at 1.9-Å resolution and identify a candidate surface for interaction with Pipe. This represents the first crystal structure of a eukaryotic protein-disulfide isomerase-related protein of the endoplasmic reticulum to be described. The dimeric protein is composed of an N-terminal thioredoxin domain and a C-terminal α-helical domain unique to protein-disulfide isomerase D proteins. Although Wind carries a C*XX*C motif that is partially surface accessible, this motif is redox inactive, and the cysteines are not required for the targeting of Pipe to the Golgi. However, both domains are required for targeting Pipe to the Golgi, and, although the mouse homologue ERp28 cannot replace the function of Wind, exchange of the Wind D-domain with that of ERp28 allows for efficient Golgi transport of Pipe.

Within the developing *Drosophila* embryo, dorsal-ventral polarity is determined by a group of 11 genes that act to create a gradient of the NFκB homologue Dorsal within the nuclei of the embryo. Dorsal is translocated to the nucleus from the cytoplasm upon activation of the transmembrane Toll receptor by an extracellular ligand, Spätzle (1). Three of the eleven genes, *i.e. nudel*, *pipe*, and *windbeutel*, are expressed in the follicle cells. Deletion of any one of these three leads to a lethal impairment in establishing dorsal-ventral polarity (2). The products of *pipe* and *windbeutel*, Pipe and Wind, are specifically required in a band of follicle cells on the ventral side of the embryo. Pipe is a Golgi-resident type II transmembrane protein with homology to mammalian heparan sulfate 2-*O*-sulfotransferase (3, 4). It is believed that Pipe modifies an as yet unidentified proteoglycan that later participates in the proteolytic activation of Spätzle in the perivitelline space. *windbeutel* is expressed in all follicle cells located over the oocyte, although it seems essential only in the ventral layer (5). Wind is an endoplasmic reticulum (ER)[1]-resident, luminal protein belonging to the protein-disulfide isomerase (PDI) family, a group of proteins with varying redox and chaperone properties (6, 7). Although the mechanism of action remains unclear, it has recently been shown that an important role for Wind is the correct targeting of Pipe to the Golgi; *windbeutel*-deficient female flies show an aberrant distribution of Pipe protein, and, when expressed in COS-7 cells, Pipe is retained in the ER in a presumably inactive form. Upon simultaneous overexpression of Wind, however, a clear redistribution of Pipe to the Golgi was observed (2).

The mammalian homologues of Wind, ERp28 (8) and ERp29 (9, 10), have been found in complexes with secretory proteins (6, 11). These proteins are members of the PDI-D subfamily of PDI-related proteins, homologues of which can be found in yeast and plants as well (6). PDI-D proteins are characterized by the presence of one or two domains of roughly 100–120 residues with sequence similarity to the thioredoxin fold of PDI, followed by a novel, α-helical region at their C terminus termed the D-domain (6).

The protein-disulfide isomerases are highly abundant proteins that catalyze the formation, reduction, and isomerization of disulfide bonds in substrate proteins, an activity dependent upon the presence of a redox-active C*XX*C tetrapeptide (7). For some of these proteins it has been shown that, in addition to their redox/isomerase activities, they can also function as chaperones (12–15).

Recent evidence has shown that many mammalian PDI-related proteins are composed entirely of thioredoxin domains (6, 16). Whereas redox function requires a C*XX*C motif, substrate binding requires primarily the redox-inactive b′ domain, although all domains are likely to participate.

In yeasts and plants, the thioredoxin domains of PDI-D proteins are redox active (these proteins are therefore termed PDI-Dα proteins) and can rescue the otherwise lethal disruption of the *pdi* gene in *Saccharomyces cerevisiae* (6, 17). Mammalian homologues, however, have a single, b-type, redox-inactive thioredoxin domain (termed PDI-Dβ proteins) (6).

* This work was supported by grants from the Deutsche Forschungsgemeinschaft (DFG) and the Fonds der Chemischen Industrie (to H.-D. S. and G. M. S.). The costs of publication of this article were defrayed in part by the payment of page charges. This article must therefore be hereby marked "*advertisement*" in accordance with 18 U.S.C. Section 1734 solely to indicate this fact.

[S] The on-line version of this article (available at http://www.jbc.org) contains Supplementary Results and Discussion, Supplementary Methods, Supplementary Figs. 1 and 2, and accompanying figure legends.

The atomic coordinates and structure factors (code 1OVN) have been deposited in the Protein Data Bank, Research Collaboratory for Structural Bioinformatics, Rutgers University, New Brunswick, NJ (http://www.rcsb.org/).

§ These two authors contributed equally to this work.

‖ To whom correspondence should be addressed. Tel.: 49-551-2011663; Fax: 49-551-2011499; E-mail: dferrar@gwdg.de.

[1] The abbreviations used are: ER, endoplasmic reticulum; GFP, green fluorescent protein; EGFP, enhanced GFP; PDI, protein-disulfide isomerase; PDI-D, PDI-related protein containing a D-domain; MES, 4-morpholineethanesulfonic acid; PEG, polyethylene glycol.

Here, we report on the successful crystal structure determination of a key component of the dorsal-ventral patterning pathway, which is also the first crystal structure of an ER-luminal, PDI-related protein. Through mutagenesis and functional assays, we identify a surface of the protein in the N-terminal b-domain that is likely to interact with Pipe. Replacement of a polar residue within this surface with a basic one severely impedes targeting of Pipe to the Golgi. In contrast, the nearby C*XX*C motif, which is redox inactive, is not required for Golgi targeting. The N-terminal domain of Wind, when expressed alone, does not promote Pipe transport to the Golgi. Furthermore, we find that although a mouse homologue of Wind, ERp28, cannot target Pipe to the Golgi, the D-domain of ERp28 can efficiently replace that of the fly protein. Thus, although the b-domain contains a site that may be involved in interaction with Pipe, the C-terminal D-domain is also required.

EXPERIMENTAL PROCEDURES

Cell Lines, Bacterial Strains, Plasmids, and Expression Vectors—COS-7 cells were purchased from the European Collection of Animal Cell Cultures, XL1-Blue bacterial cells and the pBlueScript II plasmid were from Stratagene, pEGFP-N1 was obtained from Clontech, and the pQE-30 and pQE-60 expression vectors were from Qiagen.

Antibodies and Reagents—Antibodies against *Drosophila* Wind were raised in rabbits against the recombinant, full-length, His_6-tagged protein from *Escherichia coli* according to standard procedure. IgG fractions were isolated over protein A-Sepharose from Amersham Biosciences. Rabbit antibodies against the C-terminal KEEL retrieval sequence were prepared as described elsewhere (18). Goat anti-rabbit Cy3-conjugated antibody was from Jackson ImmunoResearch Laboratories. For mutagenesis, the QuikChange site-directed mutagenesis kit from Stratagene was used. Cell culture media were from Sigma, and the Pefabloc SC protease inhibitor was purchased from Biomol.

cDNA Cloning and Expression Vector Construction—Drosophila windbeutel cDNA encoding the full-length Wind was amplified by PCR from a λZAP cDNA library (kind gift of Dr. M. Takamori, Max-Planck Institute of Biophysical Chemistry). For bacterial expression, a *Bam*HI/*Sac*I PCR product thereof, encoding mature Wind, was ligated into pQE-30, generating an N-terminal extension including a His_6 tag (MRGSHHHHHHGS). This construct is referred to as His-Wind. A further construct harboring C-terminally tagged Wind (Wind-His) was prepared by ligating a PCR-amplified transcript of Wind into the *Nco*I/*Bgl*II sites of pQE-60. Mouse ERp28 cDNA was amplified by reverse transcription PCR from F9 cells.

For expression in mammalian cells, full-length *windbeutel* was incorporated into the *Eco*RI/*Bam*HI sites of pEGFP-N1 such that a stop codon preceded the enhanced green fluorescent protein (EGFP) sequence, ensuring translation of Wind alone. A similar construct was made for ERp28. Wind point mutants (Wind-STGS, Wind-Y55K, and Wind-D31N) were constructed using appropriate primers and the QuikChange site-directed mutagenesis kit. Truncated versions of Wind encoding the N-terminal thioredoxin domain alone, with or without an appended retrieval sequence (Wind-N and Wind-N-KEEL, respectively), were constructed by PCR such that a stop codon was introduced immediately after Ser^{137} (for Wind-N) or immediately after an appended 12-bp fragment encoding the KEEL terminal retrieval sequence. A Wind-ERp28 fusion construct (Wind-N-p28D) was prepared by fusing the sequence for the C-terminal domain of mouse ERp28 (residues 149–262; Gln^{150} replaced with Ser) in-frame with that of the b-domain of Wind (residues 1–137), thereby effectively exchanging the Wind D-domain for that of mouse ERp28.

Because of difficulty in obtaining an intact Pipe transcript, *pipe* was amplified in three parts. A *Xho*I/*Xba*I fragment comprising 299 bp of the 5′-end of *pipe* (fragment 1) and an *Eco*RI/*Bam*HI fragment (fragment 4) comprising 298 bp of the 3′-end (908–1212 of *pipe*) were amplified from a *Drosophila* cDNA clone (RE11403; ResGen). An *Xba*I/*Bsm*I fragment (fragment 2) of 544 bp covering bases 300–843 of *pipe* was obtained by PCR amplification of genomic DNA from Oregon-R flies (a kind gift from Dr. M. Takamori, Max-Planck Institute for Biophysical Chemistry). All fragments were ligated into pBlueScript II. A final fragment of 64 bp (fragment 3) linking fragments 2 and 4 (bases 844–907 of *pipe*) was synthesized chemically (MWG Biotech) and used to join fragments 2 and 4 via a *Bsm*I and an introduced *Mlu*I site. The *Mlu*I site was later reverted to the original sequence to generate full-length wild-type *pipe* (1212 bp). Pipe-GFP was constructed by ligating a *Kpn*I/*Bam*HI fragment from cloned Pipe into pEGFP-N1. Expression from this construct generates a translocation-competent, full-length Pipe protein fused in-frame to the N terminus of the EGFP.

Cell Culture and Immunofluorescence Assays—COS-7 cells were grown in 90% Dulbecco's modified Eagle's medium and 10% fetal bovine serum with 2 mM L-glutamine and antibiotics at 37 °C and 10% CO_2. For immunofluorescence labeling, cells were transfected by electroporation in a Gene Pulser II device (Bio-Rad) and grown on coverslips overnight (20 h) before fixation with 4% paraformaldehyde. Wind antibody was used at a 1:150 dilution, and detection of bound antibody was performed with a 1:1000 dilution of a goat anti-rabbit Cy3-conjugated antibody. Visualization of Cy3 and GFP was carried out on an Axiovert 200 microscope (Zeiss) with filter sets with an excitation filter of 565/30 nm and 480/40 nm, a dichroic beam splitter of 595 nm and 505 nm, and emission filters of 645/75 nm and 527/30 nm, respectively.

Protein Expression and Purification—Wild-type Wind protein as well as Wind-Y55K and Wind-D31N were expressed from pQE-His-Wind and pQE-Wind-His in *E. coli* XL1-Blue cells by induction of an OD_{600} = 0.7 culture for 3 h at 37 °C with 1 mM isopropyl-1-thio-β-D-galactopyranoside. The recombinant proteins were harvested by brief sonication of lysozyme-treated cells in pH 8-adjusted phosphate buffered saline including 0.2 mM Pefabloc SC protease inhibitor followed by addition of Triton X-100 to 0.1% (v/v) and gel filtration over a nickel-nitrilotriacetic acid nickel affinity column (Qiagen). Bound protein was washed with 4 bed volumes each of wash buffer (20 mM Tris-Cl, pH 8.0, 150 mM NaCl, and 0.1% (v/v) Triton X-100) and salt wash buffer (20 mM Tris-Cl, 350 mM NaCl, and 0.1% Triton X-100), then washed again with 4 bed volumes of pre-elution buffer (20 mM Tris-Cl, pH 8.0, 150 mM NaCl, 0.01% Triton X-100, and 8 mM imidazole) and eluted in 4 bed volumes of elution buffer (20 mM Tris-Cl, pH 8.0, 300 mM NaCl, 100 mM imidazole, and 0.01% Triton X-100). Eluted protein was dialyzed extensively against dialysis buffer (10 mM HEPES, pH 7.5, 50 mM NaCl, and 0.01% (v/v) 2-mercaptoethanol), concentrated to 20–25 mg/ml, and stored at 4 °C. Protein purity was verified by 12.5% SDS-PAGE and was consistently >95% pure (for wild-type and all mutants).

Size Determination of Recombinant Protein—To estimate the molecular mass of recombinant Wind monomers/oligomers, multi-angle light scattering (19) on a DAWN DSP MALS photometer and an Optilab DSP interferometric refractometer (Wyatt Technologies) of protein separated by size exclusion chromatography on a Superdex 200 HR column (Amersham Biosciences) was performed. The protein was loaded and run in 30 mM Tris-Cl, pH 7.9, 350 mM NaCl, and 0.01% (v/v) Triton X-100 at room temperature. Results of three runs of 0.28 mg of protein each were averaged for each recombinant species.

Crystallization, Cryo Conditions, and Heavy Atom Derivatives—Crystals were grown by the hanging drop vapor diffusion method at 20 °C. The best crystals were grown by mixing 6 μl of 5.8 mg/ml Wind in 5 mM HEPES, pH 7.5, 25 mM NaCl, 0.0025% (v/v) β-mercaptoethanol with a 3-μl reservoir solution containing 0.1 M MES, pH 6.1, 0.1 M CsCl, 2 mM $CaCl_2$, and 16% (v/v) PEG 300.

0.1 M MES, pH 6.1, 0.1 M CsCl, 20% (v/v) PEG300, and 10% (v/v) glycerol was used as the cryo-protectant solution. The mercury derivative was prepared by growing crystals with a well solution of 0.1 M MES, pH 6.1, 0.08 M NaCl, 2 mM $CaCl_2$, and 16% (v/v) PEG 300 and soaking them in 0.1 M MES, pH 6.1, 0.1 M NaCl, 20% (v/v) PEG 300, 10% (v/v) glycerol, and 0.05 mM $HgCl_2$ for 2 weeks.

Data Collection and Processing—Three data sets were collected at low temperature (Table I). The data were processed by DENZO (20), SCALEPACK (20), XPREP (Bruker AXS, Madison, WI) and CCP4 (21). The crystals belong to space group C2, with two molecules in the asymmetric unit. The native data were collected on a MarCCD detector at the synchrotron beamline X11 in Hamburg at the EMBL outstation DESY. The mercury derivative and native in-house data were used for substructure determination.

Structure Solution, Refinement, and Validation—The structure was solved by single isomorphous replacement including anomalous scattering information (SIRAS). The substructure of three mercury atoms was solved and refined by a combination of difference Patterson analysis and direct methods by dual-space recycling using the program SHELXD (22) with the SIRAS data set truncated to 3.2 Å. SHELXE (23) was used for phase calculation, density modification, and phase extension. Subsequently, DM was used to do further density modification by solvent flattening and histogram matching.

The model was initially built by hand with the aid of MAID (24). Then, the partial model was extended by wARP (25). During the iterative model-building procedure, SHELXE was used for density modification to improve phases and remove model bias.

TABLE I

Statistics of the data collection and structure solution and refinement

Values in parentheses correspond to the highest resolution shell. R.m.s.d. is root mean square deviation.

	Native	Native	Mercury derivative
Data Collection			
Wavelength (Å)	0.811	1.5418	1.5418
X-ray source	X11 beamline, EMBL/DESY	Copper rotating anode	Copper rotating anode
Detector	MarCCD	Mar345	Mar345
Spacegroup	C2	C2	C2
Cell parameters (Å or °)			
a	106.678	108.107	107.998
b	50.358	50.802	50.935
c	98.616	99.030	99.122
β	112.84	112.45	112.77
Resolution limits (Å)	37.64–1.90 (2–1.90)	19.91–2.69 (2.80–2.69)	53.23–2.99 (3.10–2.99)
Reflections (unique)	38,218	13,890	10,142
Completeness (%)	99.8 (99.6)	99.0 (93.7)	99.1 (93.8)
Mean I/σ	13.96 (4.77)	21.19 (3.64)	19.29 (6.45)
Redundancy	4.50 (3.79)	7.09 (4.52)	6.75 (5.13)
R_{int}(%)[a]	5.65 (27.59)	7.12 (44.08)	6.13 (23.99)
R_{sigma}(%)[b]	4.47 (19.59)	3.88 (29)	4.28 (15.50)
Refinement statistics			
Reflections	38216		
R_{work}/R_{free} (%)[c,d]	21.58/25.57		
Protein atoms	3295		
Solvent atoms	152 water, 1 cesium		
Mean *B* value (Å^2)	37.25		
R.m.s.d. bond length (Å)	0.023		
R.m.s.d. bond angle (°)	2.13		

[a] $R_{int} = \Sigma |F_o^2 - F_o^2 (mean)|/\Sigma |[F_o^2]$.
[b] $R_{sigma} = \Sigma[\sigma (F_o^2)]/\Sigma[F_o^2]$.
[c] 5% reflections are selected in thin shells as test data set.
[d] $R_{work} = \Sigma||F_o| - |F_c||/\Sigma |F_o$ for working data set and $R_{free} = \Sigma||F_o - F_c||/\Sigma F_o$ for test data set.

The structure was refined with REFMAC5 (26) using an F-based maximum likelihood target. Model building was performed with Xfit (27), and only atoms for which electron density was visible were built into the model.

The structure was validated with PROCHECK (28). All the residues have geometry within the Ramachandran allowed region. The diagrams were produced with DINO (www.dino3d.org), MOLSCRIPT (29), and RASTER3D (30).

Protein Data Bank Accession Numbers—The coordinates and structure factors have been deposited in the Protein Data Bank with the entry code 1OVN.

RESULTS AND DISCUSSION

Overall Crystal Structure—Recombinant *Drosophila* Wind crystallizes as a homodimer (chains A and B). Each chain is composed of two distinct domains connected by a flexible linker of 11 residues (Fig. 1). The N-terminal b-domain has 118 residues and adopts an α/β fold with the order of secondary structure elements being β1-α1-β2-α2-β3-α3-β4-β5-α4. The strands of the β-sheet, with the exception of β4, have a parallel arrangement, forming a central core of all five strands surrounded by the four α-helices. This fold is characteristic for protein-disulfide isomerase and thioredoxin-related proteins (31–33). The C-terminal domain is composed of 107 residues and has a five-helix fold, termed the D-domain (6). This structure, which has all helices in anti-parallel arrangement, represents a novel fold unique to PDI-D proteins.

The residues in each monomer were numbered from 22 to 257. Residues 24–252 could be modeled for the first monomer and 23–248 for the second. The N-terminal His_6 tag sequence (MRGSHHHHHHGS) could not be seen in the density.

Oligomeric State—The crystal structure of Wind clearly shows a dimer (Figs. 1*b* and 3) formed by a head-to-tail arrangement of the N-terminal b-domains (residues 1–118) with no participation by residues within the D-domain. The dimer interface is nearly symmetric and consists primarily of residues to either side of β1 (residues 24–34), residues within and after α1 (residues 37–43), and residues within and after α2 (residues 70–75), which are involved in a mixture of hydrophobic interactions as well as hydrogen bonding. Important contributions to interface interactions from residues within and around β1 and α1 include multiple contacts between the backbone of the conserved (compared with mammalian PDI-D proteins) Gly^{26} and side-chain atoms of the conserved Asp^{31} and similar Leu^{33} residues, further interactions between a side-chain oxygen of Asp^{31} and backbone atoms of Thr^{25}, and hydrophobic interactions between the Leu^{33} and Thr^{25} residues as well as interactions between the similar Val^{28} and Ser^{34}. The side chain of Arg^{41} (lysine in ERp28/29) is involved in a series of hydrophobic contacts with Phe^{42} and Pro^{43} as well as with backbone atoms of Lys^{74} and the conserved Asp^{75} in the turn after α2. In addition, five water-mediated hydrogen bonds can be detected for residues within and around β1. The buried accessible surface area is ~758 Å^2, which corresponds to ~6.3% of the surface of the protein.

Dimerization creates a deep, hydrophilic cleft, with the approximate dimensions 11 × 11 × 27 Å between the b-domains of the monomers (see Supplementary Fig. 1 in the on-line version of this article). The cleft (hereafter referred to as the dimer cleft), which is rich in negatively charged residues, is flanked by residues from the loop between β2 and α2 and residues from the end of β3 and the following loop, with residues within and around β1 (residues 24–34) at its base. Interestingly, the CTGC motif lies at the floor near the entrance to the dimer cleft (Figs. 1 and 3), and may thus be positioned for reacting with substrate cysteines within the cleft. An electron density synthesis calculated with the derivative data shows clearly defined mercury positions (data not shown) not only for the linker cysteine of either chain but also for the first cysteine of the CTGC motif of one of the two chains (Fig. 1*b*), suggesting that these sites are freely accessible.

Superposition of the structures of the individual domains of the two chains shows excellent correlation of their three-dimensional structures with root mean square deviation values

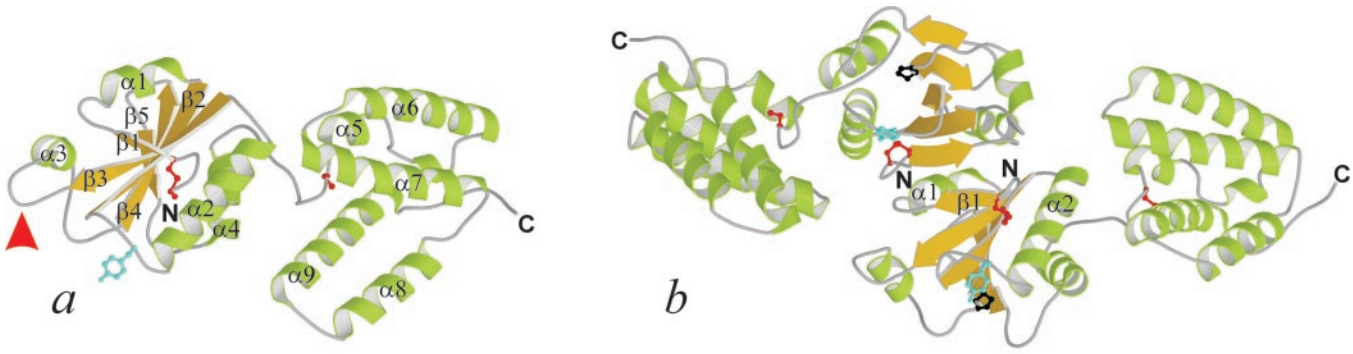

FIG. 1. **Structure of the Wind homodimer.** *a*, ribbon structure of a Wind monomer. The thioredoxin domain is shown to the *left*, the helical D-domain to the *right*. The *arrowhead* indicates the pentapeptide loop unique to PDI-Dβ proteins. The face of the thioredoxin fold shown here is partially buried in the homodimer. B-strands are colored *yellow*, helices *green*. The three cysteines are shown in *red*, Tyr^{55} in *blue*. Secondary structure elements are labeled. The monomer has the structure $\beta1$-$\alpha1$-$\beta2$-$\alpha2$-$\beta3$-$\alpha3$-$\beta4$-$\beta5$-$\alpha4$-$\alpha5$-$\alpha6$-$\alpha7$-$\alpha8$-$\alpha9$. *b*, ribbon structure of the Wind dimer. The molecule is rotated 90° compared with the monomer in *panel a*. Colors as in *panel a*. Structural elements involved in dimer interactions are labeled. Pro^{106} is shown in *black*. Dimer dimensions are ~106 × 53 × 37 Å.

for Cα coordinates of 0.61 and 0.92 Å for the b-domain and the D-domain, respectively. The difference in B-factors of 26.9 $Å^2$ between corresponding Cα atoms of the D-domains (compared with a value of 5.6 $Å^2$ between the b-domains) indicates considerable mobility within the D-domain. Interestingly, the two domains of both chains could not be superimposed simultaneously, reflecting a ~32° relative displacement of the D-domains, which could be traced to the linker region connecting the N- and C-terminal domains and primarily to rotation around the Ile^{144} and Gly^{145} residues. One consequence of this displacement is that, in the crystal, the D-domain rotates in a manner such that the gap between the tip of the D-domain (measured from Cα of Glu-226) of chain B moves from a distance of 20.6 Å to within 9 Å of the dimer cleft (measured from Glu-88).

Dimerization of Wind is also supported by multi-angle light scattering (19) measurements following size exclusion chromatography (Fig. 2), *in vitro* and *in vivo* cross-linking, and native gel analysis (data not shown) of the purified recombinant His_6-tagged protein, which suggest a dimer of 2 × 27-kDa apparent molecular mass.

The Surface above the Dimer Cleft May Be Involved in Interaction with Pipe, but Wind Dimerization May Not Be Required for Pipe Processing—Association of the monomeric subunits of Wind into the homodimer creates an electrostatically negative, elongated cleft wide enough to partially accommodate an extended polypeptide, with possible further interactions on the dimer surface surrounding the cleft and on juxtaposed regions of the D-domains. The surface around the cleft, which includes a loose cluster of three tyrosines (Tyr^{53}, Tyr^{55}, and Tyr^{86}), shows considerable conservation in PDI-Dβ homologues (Figs. 3 and 4), suggesting perhaps the presence of a common substrate-binding site. This site is close to a *cis*-proline conserved among PDI-related proteins (Fig. 5).

To investigate whether residues around the dimer cleft may be involved in interaction with Pipe, we co-expressed Pipe and Wind in COS-7 cells in which Wind was either expressed as wild-type or with a mutation within the loop before $\alpha2$ (Y55K). Tyr^{55} is surface exposed at the verge of the dimer cleft (Fig. 3) but is at least 14 Å distant from the dimer interface. Replacement with lysine was expected to disrupt the electrostatically negative surface of the dimer cleft (Fig. 3*b*) without affecting the folding of the protein. Pipe failed to exit the ER when co-expressed with Wind-Y55K (Fig. 6*j*), although the Y55K mutant is highly expressed and retained in the ER (Fig. 6, *h* and *i*), indicating that the conserved surface around Tyr^{55} and/or the surface of the dimer cleft formed by the b-domains is required for Pipe export from the ER.

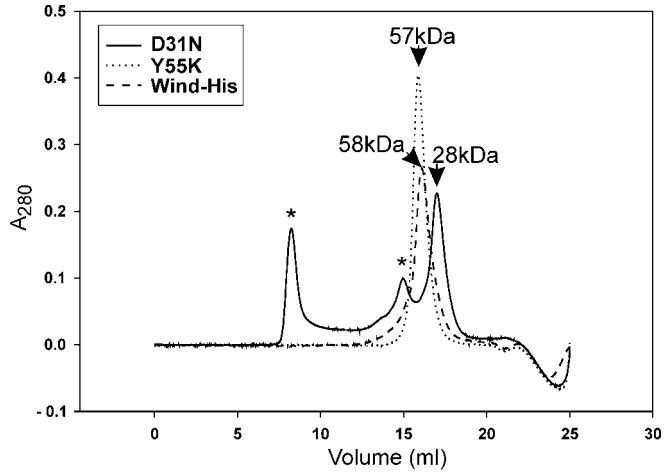

FIG. 2. **Oligomeric state of Wind.** Recombinant, His_6-tagged Wind purifies as a dimer. On a Superdex 200 HR column, Wind migrates with an apparent molecular mass of ~60 kDa similar to Wind-Y55K. In contrast, Wind-D31N migrates at ~33 kDa. For D31N, but not for Y55K, significant aggregation was observed (*asterisks*). Multi-angle light scattering of the separated peaks gave the sizes indicated above the curves. Calculated theoretical values for the proteins are 56.6 kDa (dimeric Wind-His and Wind-Y55K) and 28.3 kDa (monomeric Wind-D31N).

We can exclude the possibility that the Y55K phenotype resulted from an impaired ability of Wind to dimerize, because multi-angle light scattering assays showed a sharp peak corresponding to 57 kDa, which is virtually identical to wild-type Wind (Fig. 2). Furthermore, if the Y55K phenotype were a result of the impaired ability of Wind to dimerize, one would expect that the expression of a mutant that shows little or no dimerization should abrogate Pipe transport. To this end, we constructed a Wind mutant, D31N, which was predicted on the basis of the crystal structure to significantly impair dimer formation (Fig. 3). Indeed, D31N fails significantly to dimerize *in vitro* (Fig. 2), although it is still able, when coexpressed with Pipe in COS cells, to catalyze the translocation of Pipe to the Golgi (Fig. 6, *panels k–m*). This suggests either that a sufficient dimer can still form *in vivo* or that dimeric Wind is not necessary for Pipe processing. Thus, the lack of function of the Y55K mutant is more likely due to a direct inhibition of substrate binding rather than any impairment to dimer formation.

Both the B- and D-domains of Wind Are Required for Relocalization of Pipe, but the Function of the Wind D-domain Can Be Replaced by That of Mammalian ERp28—We asked whether the b-domain alone would be sufficient to relocate Pipe

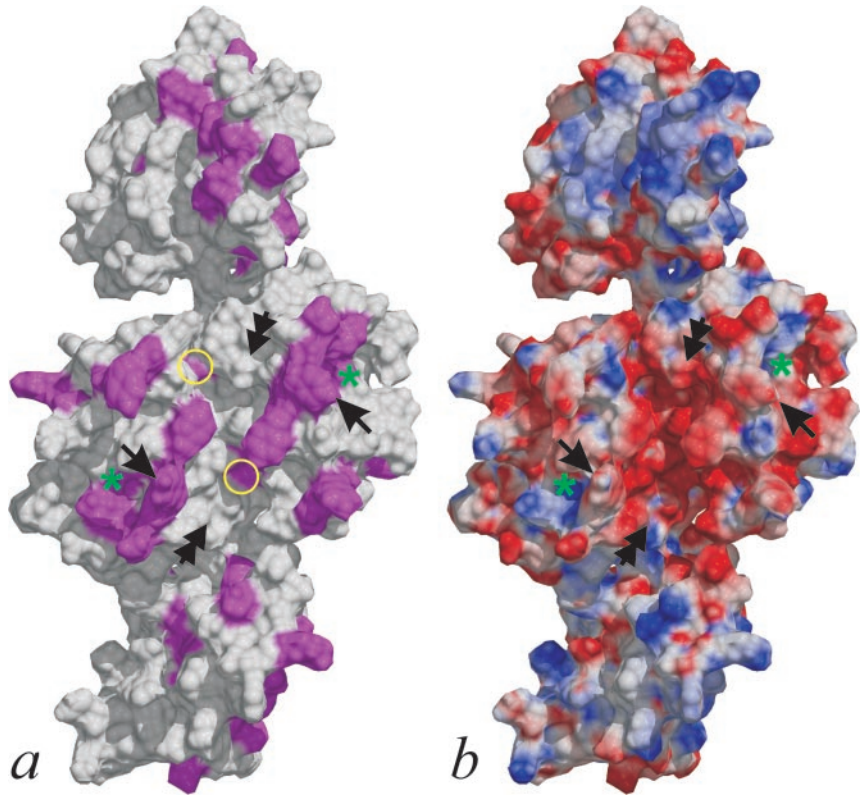

FIG. 3. **The dimer cleft is surrounded by conserved residues and contributes to the negative electrostatic potential of the surface of the b-domain.** *a*, conserved residues in PDI-Dβ proteins. Homologous residues are shown in *magenta*. Replacement of the conserved Tyr^{55} (*single arrows*) with a lysine residue abrogates Pipe transport to the Golgi, whereas replacement of both cysteines in the CTGC motif (*double arrows*) has no effect. The position of Pro^{106} is indicated with an *asterisk* and that of Asp^{31} with an *open yellow circle*. *b*, surface electrostatic potential of Wind. Negative potential is marked in *red*, positive in *blue*. Residues within the dimer cleft display a net negative electrostatic potential and may constitute a surface that interacts with substrate proteins. *Arrows* are as in *panel a*. The electrostatic surface was calculated with MEAD (45) and prepared with MSMS (46) and DINO (www.dino3d.org). Missing atoms and hydrogens were added with CNS (47).

```
                    β1          α1          β2          *           α2
Wind     22  VTCTGCVDLDEL-SFEKTVERFPYSVVKFDIAY--PYGEKHEAFTAFSKSAHKAT  73
ERp29    33  LHTKGALPLDTV-TFYKVIPKSKFVLVKFDTQY--PYGEKQDEFKRLAENSASS-  83
ERp28    35  LHTKGALPLDTV-TFYKVIPKSKFVLVKFDTQY--PYGEKQDEFKRLAENSASS-  85
PDI-a    21  EEEDHVLVLRKS-NFAEALAAHKYLLVEFYAPWCGHCKALAPEYAKAAGKLKAEG  74
PDI-b   133  -TGPAATTLPDGAAAESLVESSEVAVIGFFKD---VESDSAKQFLQAAEAI----  179

                    β3          α3          β4          β5
Wind     74  KDLLIATVGVKDYGELENKALGDRYKVDDKNFPSIFLFKGNADE-YVQLPSHVDV  127
ERp29    84  DDLLVAEVGISDYGDKLNMELSEKYKLDKESYPVFYLFRDGDFENPVPYS--GAV  136
ERp28    86  EELLVAEVGISDYGDKLNMELSEKYKLDKESYPVFYLFRDGDLENPVLYN--GAV  138
PDI-a    75  SEIRLAKVDAT-----EESDLAQQYGVR--GYPTIKFFRNGDTASPKEYT--AGR  120
PDI-b   180  DDIPFGITS--------NSDVFSKYQLD--K-DGVVLFKKFDEG-RNNFE--GEV  220

                    α4          α5          α6
Wind    128  TLDNLKAFVSANTPLYIGRDGCIKEFNEVLKNYANIPDAEQLKLIEKLQAKQEQL  182
ERp29   137  KVGAIQRWLKGQ-GVYLGMPGCLPAYDALAGQFIEASSREARQAILKQGQDGLSG  190
ERp28   139  KVGAIQRWLKGQ-GVYLGMPGCLPAYDALAGEFIKASSIEARQAILKQGQDGLLS  192
PDI-a   121  EADDIVNWLKKR                                            132
PDI-b   221  TKENLLDFIKHN                                            232

                    α7          α8
Wind    183  TDPEQQQNARAYLIYMRKIHEVGYDFLEEETKRLLRLKA  221
ERp29   191  VKETDKKWASQYLKIMGKILDQGEDFPASELARISKLIE  229
ERp28   193  VKETEKKWASQYLKIMGKILDQGEDFPASEMARIGKLIE  231

                    α9
Wind    222  -GKVTEAKKEELLRKLNILEVFRVHKVTKTAPEKEEL  257
ERp29   230  -NKMSEGKKEELQRSLNILTAFRK-----KGAEKEEL  260
ERp28   232  -NKMSDSKKEELQKSLNILTAFRK-----KEAEKEEL  262
```

FIG. 4. **Alignment of Wind against mammalian homologues and PDI.** The protein sequence of Wind (AAC-02944) was aligned against rat ERp29 (NMR data from PDB 1G7D and 1G7E, sequence accession P52555), mouse ERp28 (P57759), and PDI a- and b-domains (NMR data from PDB 1MEK, 2BJX, sequence accession P07237), based on structure. The type of secondary structure is marked at the *top*, and residues within the elements are shaded *yellow*. Identical residues are shown in *red*, similar residues are in *blue*. The partially conserved pentapeptide insert found in PDI-Dβ proteins is marked with a *black bar*. The position of Tyr^{55} is marked with an *asterisk*.

to the Golgi. To this end, we investigated the localization of Pipe in cells co-expressing a Wind construct lacking the D-domain (Wind-N, residues 1–137) as well as in cells expressing an identical construct fused to a KEEL retrieval sequence (Wind-N-KEEL). In COS-7 cells, although the Wind-N construct was poorly retained in the ER due to lack of a retrieval sequence, the Wind-N-KEEL construct was efficiently retained (Fig. 6, *n* and *q*). However, in neither case was the translocation of Pipe to the Golgi promoted (Fig. 6, *p* and *s*). This indicates that the D-domain also participates in either the folding or the transport of Pipe.

In further studies, we investigated the ability of the mouse homologue of Wind, ERp28, to functionally replace Wind in targeting Pipe to the Golgi. In our co-expression system, overexpressed full-length ERp28 failed to promote translocation of Pipe to the Golgi (data not shown). In contrast, when a fusion construct encoding the N-terminal domain of Wind linked to the D-domain of ERp28 (Wind-N-p28D) was used, an unambiguous Golgi distribution of Pipe was observed (Fig. 6*v*). Furthermore the efficiency of relocation (judged by immunofluorescence) did not differ significantly from that promoted by wild-type Wind. We conclude that, although full-length ERp28

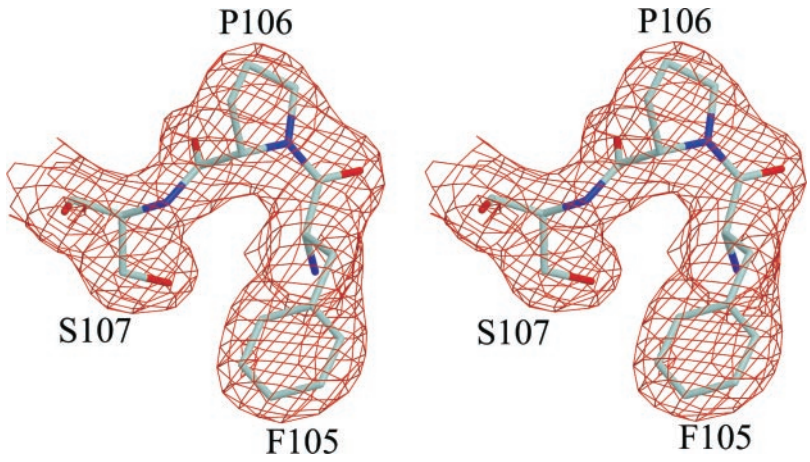

FIG. 5. **Stereo view of the electron density of Phe^{105}-Ser^{107}.** In Wind, Pro^{106} (*P106*) assumes a *cis* conformation, which is typical for corresponding residues in redox-active thioredoxin domains. *S107*, Ser^{107}; *F105*, Phe^{105}.

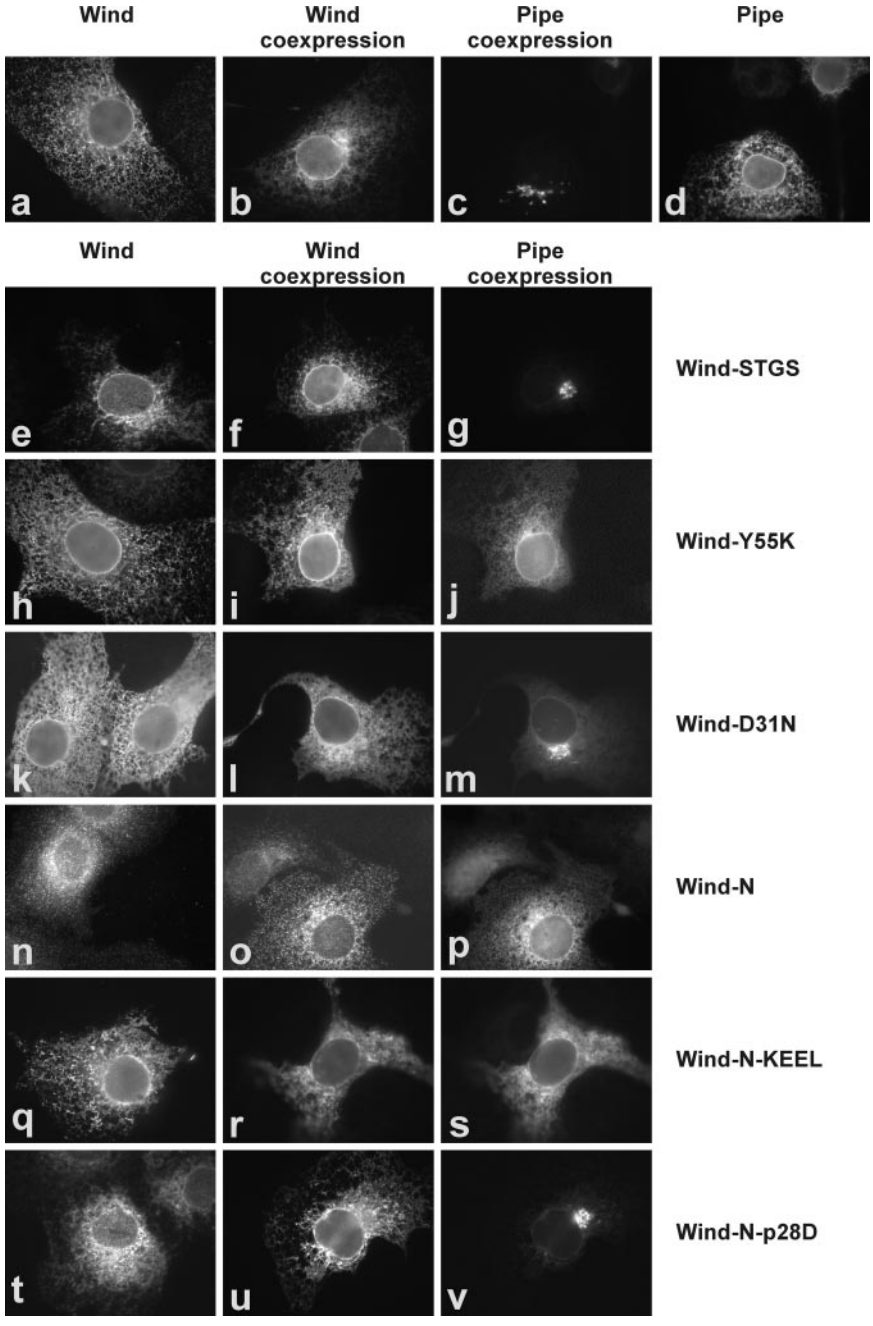

FIG. 6. **Transport of Pipe to the Golgi is abrogated in cells overexpressing a surface mutant of Wind.** In COS-7 cells expressing either wild-type Wind or Pipe-GFP, the proteins are retained in the ER (*a* and *d*) unless co-expressed, in which case Pipe-GFP is effectively translocated to the Golgi (*c*). Similar to wild-type Wind, Wind mutants Wind-STGS, Wind-Y55K, and Wind-D31N localize to the ER (*a*, *e*, *h*, and *k*), even upon co-expression of Pipe (*b*, *f*, *i*, and *l*). But whereas the replacement of the two N-terminal cysteines in Wind (Wind-STGS) has no effect on Pipe transport (*g*), Pipe fails to leave the ER in cells co-expressing Wind-Y55K (*j*). Thus it is likely that Tyr^{55} occurs on a surface that is required either for Pipe folding and/or Pipe export from the ER. Wind-N is poorly retained in the ER, both when expressed alone (*n*) and together with Pipe (*o*), and in these cells Pipe fails to reach the Golgi, being retained in the ER (*p*). Th addition of a KEEL retrieval sequence to Wind-N (Wind-N-KEEL) improves retrieval (*q* and *r*) but has no effect on Pipe sorting (*s*). In contrast, Pipe is effectively sorted to the Golgi upon co-expression of the Wind-N-p28D fusion protein (*v*). The Wind-N-p28D protein remains in the ER as expected (*t* and *u*).

cannot functionally replace Wind in relocating Pipe to the Golgi, the D-domain of ERp28 can efficiently replace the corresponding domain of Wind despite an overall identity of only 35% (~44% similarity) for the D-domains.

The CTGC Motif in Wind Is Not Essential for Pipe Transport and Lacks Catalytic Activity—Wind has a CTGC tetrapeptide at its N terminus immediately before β-strand β1. This tetrapeptide, which does not occur in PDI-Dβ homologues in other species (Fig. 4), is located within the dimer cleft ~10 Å away from Tyr^{55} and the classical site of the C*XX*C-tetrapeptide and ~20 Å from the CTGC motif of the opposite chain. In PDI, the CGHC tetrapeptide occurs at the N terminus of helix α2, which is believed to increase the reactivity of the active site (34). However, other locations also allow for redox-active dicysteine motifs, as was demonstrated for the thioredoxin-related protein DsbD (35) and other proteins that lack a thioredoxin fold (36–39).

The finding that the D-domain of ERp28 can functionally replace that of Wind, although ERp28 itself does not promote Pipe export, indicates differences in a potential substrate binding site possibly proximal to Tyr^{55}. The surface around Tyr^{55} is highly conserved (Fig. 3). One conspicuous difference is the CTGC motif in Wind located 10 Å away. To examine whether the cysteines of this motif are required for Pipe transport to the Golgi (Pipe has seven Cys residues), we engineered a mutant of Wind lacking both cysteines of the CTGC site (Wind-STGS), and investigated its ability to direct Pipe to the Golgi. No defect in localization of Pipe was observed for Wind-STGS (Fig. 6*g*) compared with COS-7 control cells transfected with wild-type, full-length *windbeutel*, and *pipe*-GFP (Fig. 6*b*). In cells lacking Wind, Pipe was retained in the ER as expected (2) (Fig. 6*d*).

Additionally, we found that Wind is unable to reduce the disulfide bond of insulin in *in vitro* reduction assays and unable to complement a *pdi*-deficient strain of *S. cerevisiae* (see Supplementary Methods and Supplementary Fig. 2 in the online version of this article), indicating that Wind lacks a general redox/isomerase activity. We conclude that the CTGC tetrapeptide of Wind is redox inactive and not required for the correct targeting of Pipe to the Golgi.

Similarities and Differences to PDI-related Proteins—Wind has a redox inactive thioredoxin domain but retains significant sequence and structural similarity with both the redox-active (a and a′) and redox-inactive (b and b′) domains of PDI. Although the PDI b-domains have diverged greatly from the a-domains and the archetypal thioredoxin domain sequence through evolution, having retained only a very low degree of homology to these domains (Fig. 4), it is becoming increasingly evident that their presence is essential not only for the redox but also for the chaperone function of PDI in the cell (7, 40).

NMR structures of both the a- and the b-domain of PDI have been reported (32, 33). Based on structural alignments, the b-domain of Wind shares 13% homology with the a-domain of human PDI and 17% homology with the a′ domain. For the PDI b-domain, the homology is ~18% (~40% similarity for all three domains) (see Fig. 4). In contrast, the degree of homology between the a- and b-domains of PDI is ~11% (44% similarity). Thus Wind (and even more so its mammalian homologue ERp28) shares a higher degree of homology to the a- and b-domains of PDI than these domains share with each other. The conserved residues are primarily within the β-strand elements of the fold or on buried faces of helices and thus are likely to serve a mainly structural role.

Superposition of the structures of the thioredoxin domains of Wind and PDI renders root mean square deviation (Cα) values of ~1.8 and ~1.5 Å for Wind and the a- and b-domains of PDI, respectively. For the a- and b-domains alone, a value of 2.1 Å was calculated. Indeed, on this basis the structure of the N-terminal domain of Wind may be somewhat closer to that of the PDI b-domain than the a-domain.

A conspicuous difference between the thioredoxin domains of Wind and PDI is the presence in Wind of an inserted pentapeptide loop (Asp^{85}-Leu^{89}) of unknown function in the turn between strand β3 and helix α3 (Fig. 1). This charged loop is surface exposed, overlooks the dimer cleft, and is partially conserved in PDI-Dβ proteins (Fig. 4).

In the b-domain of Wind, the a- and a′ domains of PDI and other PDI-like proteins as well as in thioredoxins, a conserved *cis*-proline (Pro^{106} in Wind) is positioned near strand β4 (Figs. 4 and 5). This proline has been suggested to form part of a hydrophobic substrate-binding site close to the active site in thioredoxin-like proteins (41), and its *cis* conformation is important for maintaining the integrity of the thioredoxin fold. In Wind as well, this surface shows some hydrophobic character due mainly to a cluster of exposed, conserved tyrosines (Tyr^{53}, Tyr^{55}, and Tyr^{86}), is partially conserved in other PDI-Dβ proteins (Fig. 3*a*), and may be involved in substrate binding. The PDI b-domain, however, lacks a corresponding *cis*-proline. Thus, the structure of the b-domain of Wind seems to be intermediary between those of the PDI a- and b-domains.

Recently, NMR-structures of the individual domains of rat ERp29 were reported (42). Although the thioredoxin domain *per se* shows good correlation with the thioredoxin domain of Wind (root mean square deviation for coordinates of 2.6 Å), the dimerization interface suggested by NMR and that suggested by our crystal structure are on the opposite sides of the thioredoxin domain. Furthermore, in ERp29, the proline residue corresponding to Pro^{106} was found to be *trans*.

Additionally, we were unable to superimpose our crystal structure of the D-domain over the one suggested by NMR. In the NMR structure, helixes 8 and 9 are ~90° displaced from the position of the corresponding helices in Wind and have a relative rotation of ~30° about their common axis. For Wind, such a movement would expose several hydrophobic residues within the core of the domain and is unlikely to occur. We have shown here that the D-domain of mouse ERp28 can functionally replace the corresponding domain of Wind when expressed as a fusion protein, indicating that the structure of the D-domain of ERp28 (and thus of rat ERp29) is more likely similar to that of the D-domain of Wind. However, it is clear that the D-domain does display some flexibility, which is not only suggested by the difference in B-factors of 26.9 $Å^2$ between the D-domains of the two monomeric subunits but also by the relative movements of the two domains, amounting to >30°, seen when the two domains are superimposed. Taking into consideration the low overall similarity between Wind and ERp29 (44% similarity, 33% identity), some species-specific differences in dimerization and structure cannot be ruled out.

Conclusion—Wind is a key factor in triggering dorsal-ventral patterning in *Drosophila*. An indication of its function was provided by Stein and co-workers (2), who found a requirement for Wind in the transport of the Golgi-resident Pipe protein from the ER to the Golgi.

The most conserved surface of Wind surrounds a deep cleft formed by homodimerization of the b-domains. We can show that replacement of a conserved, polar residue at the top of the cleft with a basic one (Y55K), which does not impair dimer formation *in vitro*, completely abrogates Pipe transport. Tyr^{55} is located in a loose cluster of conserved, solvent-exposed tyrosine residues (Tyr^{53}, Tyr^{55}, and Tyr^{86}) in the turn before helix α2, corresponding to the position of the active site CGHC tetrapeptide in PDI. In fact, it now seems that all three tyrosines, as well as nearby residues around and within the dimer cleft,

may be involved in the processing of Pipe.[2] Whether Wind dimer formation is required for Pipe processing remains to be verified; Wind D31N, which exists primarily as a monomer *in vitro*, still supports Pipe processing *in vivo*. This may either be due to a small amount of dimer still being formed, or dimer formation may not be required at all. Providing a direct interaction with Pipe occurs, substrate binding may occur at least in part via the conserved surface of Wind in the vicinity of Tyr^{55}, perhaps also with participation of the negatively charged dimer cleft (or the corresponding surfaces in monomeric Wind).

In Pipe (GenBank™ accession number NP_524158), a region predicted to be within the luminal domain (Ser^{96}-Asn^{139}) shows a high content of basic residues (pI, 11.3) distinct from other, more C-terminally located sequences with net negative charge. If this were to reflect a binding surface for Wind, the case could be somewhat analogous to that suggested for the interaction of the sarcoplasmic reticulum protein Calsequestrin with the membrane protein Junctin (43, 44). One may speculate that Pipe might bind in part via its positively charged residues to electrostatically negative surfaces of Wind within or near the dimer cleft and, in part, with (more hydrophobic?) contacts on the conserved surface around Tyr^{55}. This interaction may compete with the homo-oligomerization of Pipe in the ER via its acidic and basic domains, thereby freeing the Pipe polypeptide and rendering it transport competent.

Perhaps reflecting functional conservation, the structure of the PDI-D protein Wind is the closest fit known, to date, to the NMR structures of the a- and b-domains of PDI. One trait that many of the PDI-related proteins have in common with the b-domain of Wind is the low pI of their thioredoxin fold domains. Thus the structure of Wind, in conjunction with a more detailed mapping of its substrate-binding site, may also give useful insights into peptide binding properties and structure/function relationships of a- and b-domains in PDI and other PDI-related proteins.

Acknowledgments—We are grateful to Markus Wahl for assistance with Fig. 3*b* and Reinhard Jahn for critical reading of the manuscript.

REFERENCES

1. Belvin, M. P., and Anderson, K. V. (1996) *Annu. Rev. Cell Dev. Biol.* **12,** 393–416
2. Sen, J., Goltz, J. S., Konsolaki, M., Schupbach, T., and Stein, D. (2000) *Development* **127,** 5541–5550
3. Sergeev, P., Streit, A., Heller, A., and Steinmann-Zwicky, M. (2001) *Dev. Dyn.* **220,** 122–132
4. Kobayashi, M., Habuchi, H., Yoneda, M., Habuchi, O., and Kimata, K. (1997) *J. Biol. Chem.* **272,** 13980–13985
5. Konsolaki, M., and Schupbach, T. (1998) *Genes Dev.* **12,** 120–131
6. Ferrari, D. M., and Söling, H. D. (1999) *Biochem. J.* **339,** 1–10
7. Freedman, R. B., Klappa, P., and Ruddock, L. W. (2002) *EMBO Rep.* **3,** 136–140
8. Ferrari, D. M., Nguyen Van, P., Kratzin, H. D., and Soling, H. D. (1998) *Eur. J. Biochem.* **255,** 570–579
9. Demmer, J., Zhou, C., and Hubbard, M. J. (1997) *FEBS Lett.* **402,** 145–150
10. Mkrtchian, S., Fang, C., Hellman, U., and Ingelman-Sundberg, M. (1998) *Eur. J. Biochem.* **251,** 304–313
11. Sargsyan, E., Baryshev, M., Szekely, L., Sharipo, A., and Mkrtchian, S. (2002) *J. Biol. Chem.* **277,** 17009–17015
12. McLaughlin, S. H., and Bulleid, N. J. (1998) *Biochem. J.* **331,** 793–800
13. Cai, H., Wang, C. C., and Tsou, C. L. (1994) *J. Biol. Chem.* **269,** 24550–24552
14. Wang, L., Fast, D. G., and Attie, A. D. (1997) *J. Biol. Chem.* **272,** 27644–27651
15. Gillece, P., Luz, J. M., Lennarz, W. J., de La Cruz, F. J., and Romisch, K. (1999) *J. Cell Biol.* **147,** 1443–1456
16. Kemmink, J., Darby, N. J., Dijkstra, K., Nilges, M., and Creighton, T. E. (1997) *Curr. Biol.* **7,** 239–245
17. Monnat, J., Neuhaus, E. M., Pop, M. S., Ferrari, D. M., Kramer, B., and Soldati, T. (2000) *Mol. Biol. Cell* **11,** 3469–3484
18. Majoul, I. V., Bastiaens, P. I. H., and Söling, H. D. (1996) *J. Cell Biol.* **133,** 777–789
19. Wyatt, P. J. (1993) *Anal. Chim. Acta* **272,** 1–40
20. Otwinowski, Z., and Minor, W. (1997) *Methods Enzymol.* **276,** 307–326
21. Collaborative Computational Project Number 4 (1994) *Acta Crystallogr. Sect. D Biol. Crystallogr.* **50,** 760–763
22. Sheldrick, G. M., Hauptman, H. A., Weeks, C. M., Miller, M., and Usón, I. (2001) in *International Tables for Crystallography* (Arnold, E., and Rossmann, M. G., eds) Vol. F, pp. 333–351
23. Sheldrick, G. M. (2002) *Z. Kristallogr.* **217,** 644–650
24. Levitt, D. G. (2001) *Acta Crystallogr. Sect. D Biol. Crystallogr.* **57,** 1013–1019
25. Perrakis, A., Morris, R., and Lamzin, V. S. (1999) *Nat. Struct. Biol.* **6,** 458–463
26. Murshudov, G. N., Vagin, A. A., and Dodson, E. J. (1997) *Acta Crystallogr. Sect. D Biol. Crystallogr.* **53,** 240–255
27. McRee, D. E. (1999) *J. Struct. Biol.* **125,** 156–165
28. Laskowski, R. A., MacArthur, M. W., Moss, D. S., and Thornton, J. M. (1993) *J. Appl. Crystallogr.* **26,** 283–291
29. Kraulis, P. J. (1991) *J. Appl. Crystallogr.* **24,** 946–950
30. Merrit, E. A., and Murphy, M. E. P. (1994) *Acta Crystallogr. Sect. D Biol. Crystallogr.* **50,** 869–873
31. Katti, S. K., LeMaster, D. M., and Eklund, H. (1990) *J. Mol. Biol.* **212,** 167–184
32. Kemmink, J., Darby, N. J., Dijkstra, K., Nilges, M., and Creighton, T. E. (1996) *Biochemistry* **35,** 7684–7691
33. Kemmink, J., Dijkstra, K., Mariani, M., Scheek, R. M., Penka, E., Nilges, M., and Darby, N. J. (1999) *J. Biomol. NMR* **13,** 357–368
34. Kortemme, T., Darby, N. J., and Creighton, T. E. (1996) *Biochemistry* **35,** 14503–14511
35. Katzen, F., Deshmukh, M., Daldal, F., and Beckwith, J. (2002) *EMBO J.* **21,** 3960–3969
36. Langenbach, K. J., and Sottile, J. (1999) *J. Biol. Chem.* **274,** 7032–7038
37. O'Neill, S., Robinson, A., Deering, A., Ryan, M., Fitzgerald, D. J., and Moran, N. (2000) *J. Biol. Chem.* **275,** 36984–36990
38. de Crouy-Chanel, A., Masamichi, K., and Richarme, G. (1995) *J. Biol. Chem.* **270,** 22669–22672
39. Richarme, G. (1998) *Biochem. Biophys. Res. Commun.* **252,** 156–161
40. Klappa, P., Ruddock, L. W., Darby, N. J., and Freedman, R. B. (1998) *EMBO J.* **17,** 927–935
41. Nordstrand, K., Aslund, F., Holmgren, A., Otting, G., and Berndt, K. D. (1999) *J. Mol. Biol.* **286,** 541–552
42. Liepinsh, E., Baryshev, M., Sharipo, A., Ingelman-Sundberg, M., Otting, G., and Mkrtchian, S. (2001) *Structure* **9,** 457–471
43. Zhang, L., Kelley, J., Schmeisser, G., Kobayashi, Y. M., and Jones, L. R. (1997) *J. Biol. Chem.* **272,** 23389–23397
44. Wang, S., Trumble, W. R., Liao, H., Wesson, C. R., Dunker, A. K., and Kang, C. H. (1998) *Nat. Struct. Biol.* **5,** 476–483
45. Bashford, D. (1997) in *Scientific Computing in Object-Oriented Parallel Environments* (Ishikawa, Y., Oldehoeft, R. R., Reynders, J. V. W., and Tholburn, M., eds) Vol. 1343, ISCOPE97 Ed., pp. 233–240, Springer, Berlin
46. Sanner, M. F., Olson, A. J., and Spehner, J. C. (1996) *Biopolymers* **38,** 305–320
47. Brunger, A. T., Adams, P. D., Clore, G. M., DeLano, W. L., Gros, P., Grosse-Kunstleve, R. W., Jiang, J.-S., Kuszewski, J., Nilges, N., Pannu, N. S., Read, R. J., Rice, L. M., Simonson, T., and Warren, G. L. (1998) *Acta Crystallogr. Sect. D Biol. Crystallogr.* **54**, 905–921

[2] K. Barnewitz, C. Guo, S. Verrier, H.-D. Söling, and D. M. Ferrari, manuscript in preparation.

Protein Structure and Folding:

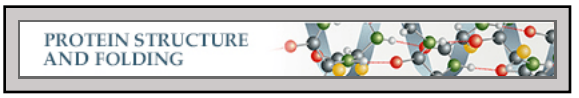

Crystal Structure and Functional Analysis of *Drosophila* Wind, a Protein-disulfide Isomerase-related Protein

Qingjun Ma, Chaoshe Guo, Kathrin Barnewitz, George M. Sheldrick, Hans-Dieter Söling, Isabel Usón and David M. Ferrari

J. Biol. Chem. 2003, 278:44600-44607.
doi: 10.1074/jbc.M307966200 originally published online August 26, 2003
